Optimization of a six-zone simulated moving bed chromatographic process

Lim, Young-il; Jørgensen, Sten Bay

Published in:
Industrial & Engineering Chemistry (I&EC) Research

Link to article, DOI:
10.1021/ie0613772

Publication date:
2007

Optimization of a six-zone simulated moving bed chromatographic process

Young-Il Lim[*] and Sten Bay Jørgensen[†]

[*] Department of chemical engineering, Hankyong National University, Anseong, 456-749 Korea

[†] CAPEC, Department of chemical engineering, Technical University of Denmark, 2800 Kgs. Lyngby, Denmark

Abstract

Using strong cation exchange simulated moving bed (SMB) chromatography, a nitrogen-phosphate-potassium (NPK) fertilizer is produced in a cost-effective manner. The SMB process operated in a non-traditional way is divided into production and regeneration sections for exclusion of undesirable ions, and composed of six zones including two wash-water zones. This paper addresses modeling, simulation and optimization studies on this ion-exchange SMB process, based upon experimental data obtained both from a pilot plant and an industrial plant.

Model parameters which are initialized by empirical equations are identified, comparing simulation results with the experimental data. Through sensitivity analysis of the model parameters, their effects on the process performance are examined. The simulation results show good agreement with *in situ* experimental data obtained in both the pilot and industrial scale plants.

This study aims to optimize the SMB process in terms of i) maximization of productivity in the production section and ii) minimization of wash-water consumption, thereby resulting in i) increasing the profit and ii) reducing the overall operating cost in the downstream processing, respectively. The two objectives are sequentially treated within the framework of a multi-level optimization procedure (MLOP) which includes two pre-optimization levels, a productivity maximization level and a desorbent (or wash-water) consumption minimization level. In this optimization study, it is demonstrated that wash-water consumption can be reduced by 5 % at a 5% higher productivity.

Keywords: Chromatographic separation, Ion-exchange simulated moving bed (SMB), NPK fertilizer, Simulation and Optimization, Parameter sensitivity.

[*] Corresponding author, phone: +82 31 670 5207, fax: +82 31 670 5445, email: limyi@hknu.ac.kr.

1. Introduction

Simulated moving bed (SMB) chromatography is a powerful technique to continuously separate multiple components in large amounts and is useful for a preparative scale. Thus, the SMB process constitutes an interesting alternative to conventional batch chromatography and has recently gained an increased impact.[1] The SMB chromatography usually works with the inherent advantage of a high driving force, resulting in low solvent consumption, small apparatus scale and high yields. However, in order to fully take advantage of this principle, a large number of operational parameters (e.g., flowrates, switching time and column configuration) need to be properly adjusted.[2]

For mathematical modeling and computer simulation of SMB systems, several different models are used, including true moving bed (TMB) model,[3-4] continuous moving bed (CMB) model for linear systems[5-6] and simulated moving bed (SMB) model[1,7-8]. However, the quality of the solution of the TMB or CMB model is only sufficient for a restricted range of applications.[1] The SMB model with periodic port movement in the flow direction is more realistic than the TMB or CMB models[5] but requires a longer calculation time.[9] However, the SMB model with periodic port movement may not be suitable for repeated runs in optimization procedures.[4]

A packed-bed chromatographic separation can be described by convection-dominated parabolic partial differential equations (PDEs) for mass conservation in the mobile phase, ordinary differential equations (ODEs) for the solute adsorption in the stationary phase, and eventually algebraic equations (AEs) for the adsorption isotherm between the two phases. Thus, the combined models lead to a nonlinear and coupled partial differential algebraic equation (PDAE) system which is often solved, after discretization of spatial derivatives, by ODE or DAE (differential algebraic equation) time-integrators (e.g., DASSL[10]) in the framework of the method of lines (MOL).[4-5,8,11-13] The MOL converts the distributed dynamic system into a large system of ODEs or DAEs, which often requires a long computational time and may give rise to substantial discretization error.[14]

A conservation element and solution element method,[14-17] CE/SE method for short, has been proposed to accurately and effectively solve the distributed dynamic system (or PDEs). The CE/SE method enforces both local and global flux conservation in space and time by using the Gauss's divergence theorem, and uses a simple stencil structure (two points at the previous time level and one point at the present time level) that leads to an explicit time-marching scheme.[17]

A nitrogen-phosphate-potassium (NPK) fertilizer process has been designed and operated by Kemira Denmark A/S in a cost-effective manner using simulated moving bed (SMB) chromatography packed with a strong cation-exchange resin ($D_c \times L_c$ = 2m×1.8m, 16 columns). This SMB process exhibits several characteristic features: i) the

feed solution is a strong electrolyte, i.e., acid solution of about 10 eqv/l (=equivalent mole/l) with nonlinear adsorption isotherms, ii) a non-equilibrium adsorption model should be considered due to a strong mass transfer effect within large resin particles, iii) it contains six zones including two wash-water zones for ion-exclusion which divide the process into production and regeneration sections (see Fig. 1), iv) the process with 16 columns is pre-operated for 5 hours with a switching time of 5 min to reach a cyclic stationary state, v) steep or discontinuous concentration profiles appear in several places and vi) a modest purity requirement of the resulting product solution is sufficient to minimize losses of valuable components. The features i)-iii) and vi) render this SMB process non-standard, thus a model is developed to investigate different aspects of this SMB operation and to optimize the process. A nonlinear and nonequilibrium SMB model[1,7-8] is developed in this study and the CE/SE method[14,17] is employed to ensure fast and accurate calculation.

This article reports both experimental and simulation studies on the non-traditional ion-exchange SMB process for chloride-free NPK fertilizer production[18]. The study aims to optimize the SMB process in order to reduce wash-water consumption and to increase productivity within a given purity, which will result in reducing the operating cost of downstream evaporation and drying processes.

The remainder of the paper is organized as follows. Section 2 describes the specific SMB process. Section 3 presents mathematical models and model parameters. Simulation and optimization results are analyzed in section 4 by comparison with experimental data. The conclusions are drawn in section 5.

2. Process description

While conventional NPK (Nitrogen-Phosphate-Potassium) fertilizers usually contain large amounts of chloride arising from the introduction of the necessary potassium content as *KCl,* the Ca^{2+}-H^{+}-K^{+} ion-exchange SMB process operated at Kemira A/S in Denmark had been designed to produce chloride-free fertilizer.[18] The raw materials normally used in the manufacturing of NPK fertilizers are nitric acid for nitrogen (N), calcium phosphate for phosphate (P) and potassium chloride for potassium (K). The two unwanted elements are calcium and chloride. Calcium is removed by cation-exchange between Ca^{2+} and K^{+} and the chloride as an anion is excluded from the product by separating the production section from the regeneration section.

A cation exchange reaction between counter-ions Ca^{2+}, H^{+} and K^{+} takes place on a strong cation-exchange resin (macroporous Purolite 160C, $d_p = 0.675 \times 10^{-3} m$, average pore diameter=$1.0 \times 10^{-7}$ m):

$$Ca^{2+}_{(aq)} + 3K \cdot R_{(resin)} + H^{+}_{(aq)} \leftrightarrow Ca \cdot R_{2\,(resin)} + H \cdot R_{(resin)} + 3K^{+}_{(aq)} \quad (1)$$

In Fig. 1, a 16-column arrangement is shown. There are two feed solutions (TS and TK), two wash water solutions (V1 and V2), product and regenerated solutions (FS and KK) and two slip water solutions (SV and KV). KV is totally recycled to V1. It is important that operating conditions are adjusted such that the KV stream does not contain ions (e.g., Ca^{2+} and Cl^-). SV is only used for back-washing (BW). The back-washing column serves to remove nitrate ions and to clean the resin particles which could be contaminated by the feed solution impurities. After one cycle period, all positions are shifted in the direction of the liquid flow. For this SMB system, several rounds (1 round=16 shiftings) are required to reach a periodic stationary state[7].

In the production section (V1-TS-FS-SV) which includes Zone I-II-III, calcium and hydrogen ions (Ca^{2+}-H^+) are removed from the feed solution which contains dissolved phosphate rock with nitric acid (TS), through adsorption of Ca^{2+} and H^+ on the resin. At the same time, potassium ions (K^+) are desorbed from the resin. Hence, the product solution (FS) contains the three desired components NPK (NO_3^-, PO_4^{3-}, K^+). In the regeneration section (V2-TK-KK-KV) which includes Zone IV-V-VI, the adsorbed calcium and hydrogen ions ($Ca^{2+} - H^+$) are replaced by potassium ions through feeding the KCl solution (TK). For simplicity, the ternary system is considered as a binary system, assuming that the first component is Ca^{2+}-H^+ and the second component is K^+. This simplifying assumption is reasonable in practice because the main objective of the process is to add K^+ into the feed solution (TS), while removing both Ca^{2+} *and* H^+. The purity of K^+ in the FS solution is one of the most important indicators for the process performance.

The backwashing column (BW) is not modeled in this simulation study. In the model development described below 15 columns are considered. These are grouped into 6 zones such as wash water Zone I (3 columns), production Zone II (3 columns), slip water Zone III (3 columns), another wash water Zone IV (1 column), regeneration Zone V (4 columns) and another slip water Zone VI (1 column), as shown in Fig. 1. The column configuration is described by the number of columns for each zone, expressed as [3/3/3-1-1/4/1], which is a typical column configuration for the industrial-scale plant. However various modified column configurations are possible. The six-zone SMB process is different from a traditional four-zone SMB process in a sense that there exist two wash-water zones (zone I and IV in Fig. 1) to enable Cl^--free and NO_3^--free operation in the production and regeneration sections, respectively. Therefore, the SMB process can be considered as ion-exclusion and ion-exchange chromatography.

Typical design parameters, operating conditions and simulation parameters are reported in Tables 1 and 2 for two ion-exchange SMB plants; one at pilot- and another at industrial-scale, respectively. The pilot plant is designed for identifying optimal operating conditions to be implemented in the real plant. The same feed solution and the same

resin type are used in the two plants, which normally are operated at the same shifting time ($\tau = 5\,min$). The production capacity of the real plant is about 500 times higher than that of the pilot plant. Despite the quite different column diameter of the two plants, the operation is carried out at a similar interstitial velocity.

Eq. (1) shows the exothermic adsorption reaction. For adsorption columns, e.g., zone II in Fig. 1, the temperature varies $45 \le T \le 55\ ^oC$ but the average temperature is assumed as $T = 50^oC$. The resin capacity on the basis of the bed volume ($n_T = 2.0 \pm 0.1\ eqv/l$) is experimentally confirmed. Since the resin concentration (n) is often expressed on the basis of the resin particle volume including the pore volume (see Eq. (2) in section 3), the resin capacity on the basis of the resin volume ($n_{T,p}$) is shown in Tables 1 and 2. In the following section, a simulated moving bed model and the model parameters in Table 1 and 2 are detailed.

3. Model development

When mass transfer resistance in the particle is significant for the adsorption mechanism because of the large resin particle diameter, a non-equilibrium model can be employed for chromatographic column models. A packed-bed chromatographic adsorption between the stationary and mobile phases for each cation (i.e., Ca^{2+}, H^+ and K^+) leads to a partial differential algebraic equation (PDAE) system involving one partial differential equation (PDE), one ordinary differential equation (ODE) and one algebraic equation (AE). The chromatographic column model is:

$$\frac{\partial C}{\partial t} + \frac{\partial (v_L \cdot C)}{\partial z} = \frac{\partial}{\partial z}\left(D_{ax} \frac{\partial C}{\partial z} \right) - \frac{1-\varepsilon_b}{\varepsilon_b} k(n^* - n) \tag{2a}$$

$$\frac{dn}{dt} = k(n^* - n) \tag{2b}$$

$$0 = n^* - g(C) \tag{2c}$$

where v_L is the interstitial velocity, D_{ax} is the axial dispersion coefficient and ε_b is the bed voidage. The liquid and solid concentrations for each component are C and n, respectively. n^* is the equilibrium concentration that is normally defined as a function $g(C)$ of the liquid concentration. A conventional linear driving force (LDF) model with a lumped mass transport coefficient (k) is employed in Eq. (2b) for the adsorption kinetics. The Peclet ($Pe = \frac{v_L L_c}{D_{ax}}$) and the Stanton ($St = \frac{kL_c}{v_L}$) numbers are the important dimensionless groups that determine in the numerical characteristics steepness of the concentration profiles and stiffness of the equation system, respectively. For example, when Pe is large and St is small, the system will exhibit steep gradients in the spatial direction (z)

and non-stiff in time (t). In Eq. (2), two initial conditions (IC, $t=0$) for two time derivatives and two boundary conditions (BC, z=0 or L_c) for the convection and diffusion terms are required.

$$IC = \begin{cases} C(z,0) = C_{initial}\ (t = 0, \forall z) \\ n(z,0) = n_{initial}\ (t = 0, \forall z) \end{cases} \tag{3}$$

$$BC = \begin{cases} v_L\left(C_{z=0} - C_{in}\right) = D_{ax}\left.\dfrac{\partial C}{\partial z}\right|_{z=0}, \ \forall t \\ \left.\dfrac{\partial C}{\partial z}\right|_{z=L_c} = 0, \forall t \end{cases} \tag{4}$$

where, C_{in} is the inlet concentration entering the column, which is given by the operating conditions.

The SMB process is modeled by connecting the column model, Eqs. (2), (3) and (4), with the node model which represents the periodic operation through the port switching.[7] Inlet concentrations (C_{in}) and a flowrate (Q_{in}) for each column are calculated from the outlet concentration (C_{out}^{node}) and flowrate (Q_{out}^{node}) in the node where perfect mixing is assumed (see Fig. 2):

$$\begin{aligned} Q_{in} \equiv Q_{out}^{node} &= Q_{in}^{node} + \alpha_1 Q_{V1} + \alpha_2 Q_{TS} + \alpha_3 Q_{V2} + \alpha_4 Q_{TK} - \alpha_5 Q_{FS} - \alpha_6 Q_{KK} \\ C_{in} \cdot Q_{in} = C_{in}^{node} \cdot Q_{in}^{node} &+ \alpha_1 C_{V1} \cdot Q_{V1} + \alpha_2 C_{TS} \cdot Q_{TS} + \alpha_3 C_{V2} \cdot Q_{V2} + \alpha_4 C_{TK} \cdot Q_{TK} - \alpha_5 C_{in}^{node} \cdot Q_{FS} - \alpha_6 C_{in}^{node} \cdot Q_{KK} \end{aligned}$$

(5)

where α_1-α_6 are the logical variables (0 or 1) according to the port switching. Fig. 2 (a) depicts a node connecting two columns. The flowrate (Q_{out}^{node}) calculated from the node model determines the flowrate (Q_{in}) of the next column. The outlet concentration from the node model is the inlet concentration (C_{in}) to the next column. Thus this node model together with the switching policy describes the SMB operations model. The two boundary conditions, Eq. (4), are employed at the inlet and outlet of each column, as shown in Fig. 2 (b).

The SMB model contains several model parameters such as bed voidage (ε_b), axial dispersion coefficient (D_{ax}), mass transfer coefficient (k) and adsorption isotherms (n^*), which may be determined through experiments or empirical models.

The bed voidage (ε_b) is mainly related to particle packing characteristics in the column. However, in SMB plants considerable extra-column volume (or dead volume) including distributors, collectors, connecting pipes and valves can be involved.[4,20] Beste et al. (2000)[4] introduce an effective column length and effective bed voidage:

$$L_{c,\,eff} = \frac{V_{total}}{S} = L_c + \frac{V_{dead}}{S} \tag{6}$$

$$\varepsilon_{b,\,eff} = \frac{V_{liquid}}{V_{total}} = \frac{\varepsilon_b L_c S + V_{dead}}{L_c S + V_{dead}} \tag{7}$$

The bed voidage (ε_b=*0.37*) is assumed to be constant, ignoring resin shrinking and swelling effects during desorption and adsorption. The two effective values are substituted for L_c and ε_b in Eqs. (2)-(4). The effective bed voidage ($\varepsilon_{b,eff}$) is larger than the bed voidage (ε_b) and the resin particles are distributed less densely in simulation but to the same extent as in reality.

The axial dispersion coefficient (D_{ax}) does not have a substantial effect on the solution of the model in general. However, axial dispersion will be larger than an expected value obtained from an empirical model for the single column, considering that backmixing is substantial in the connecting zones between columns.[19] In this study, the axial dispersion coefficient is estimated for the pilot plant[19]:

$$D_{ax}=0.02 \cdot v_L \tag{8}$$

for the real plant[19],

$$D_{ax}=0.04 \cdot v_L \tag{9}$$

On the basis of these values, the axial Peclet numbers ($Pe = \frac{L_{c,eff} \cdot v_L}{D_{ax}}$) are about 105 and 65 for the two plants.

It is considered that the Ca^{2+}-H^+-K^+ ion-exchange adsorption mechanism is controlled by the intra-particle diffusion resistance rather than the liquid film resistance, as the diameter of the resin particles used is large. The linear driving force model is employed in this study for the intra-particle diffusion (Eq. 2 (b)). The mass transfer coefficient is set to $k_{prod} = 0.4\,min^{-1}$ for the production section and $k_{regen} = 0.7\,min^{-1}$ for the regeneration section.[19] The Stanton number ($St = \frac{kL_{c,eff}}{v_L}$) varies $1.4 \le St \le 5.8$ for the two plants. The sensitivity of the process performance to the model parameters will be analyzed in section 4.

3.1 Generalized adsorption rate model

As mentioned earlier, two wash water zones (zone I and IV in Fig. 1) are arranged in the present SMB plants to achieve Cl^--free and NO_3^--free operation. The wash-water zones can become a non-adsorption region (or reach a quasi-equilibrium state between the liquid and solid phases), when the resin contacts with the aqueous solution containing negligible concentration of cations (e.g., $pH = 6 \sim 7$). Thus both non-equilibrium regions (adsorption regions) and equilibrium regions (non-adsorption regions) are present in the NPK SMB unit.

The LDF model represents intrinsically non-equilibrium adsorption, since the actual resin concentration (n_i) can not reach the equilibrium concentration (n_i^*) because of the mass transfer rate (k). When adsorption kinetics has a very large mass transfer rate (k), the LDF model is close to an equilibrium model. The difference between the two

concentrations ($n_i^* - n_i$) is however large for a small mass transfer rate (k) as in this NPK fertilizer process. A dual adsorption kinetics model may therefore be needed as follows:

$$r_i \equiv \frac{dn_i}{dt} = k(n_i^* - n_i) \quad for \;\; adsorption \;\; regions \tag{10a}$$

$$r_i \equiv \frac{dn_i}{dt} = 0 \quad for \; nonadsorption \; regions \tag{10b}$$

The switch between the above two adsorption rate models presents a state change (or event) whenever a state condition is satisfied. The state condition of the present ion-exchange SMB system is determined by the presence of cations in the fluid. If there is no cation in the fluid, adsorption or desorption does not occur as shown in Eq. (10b). This problem shows a behavior which is analogous to that of a heat conduction problem[21] where a material undergoes a phase change at different spatial positions in time.

The discrete events in the partial differential algebraic equation (PDAE) system for the SMB process move temporally and spatially. Consequently it is a challenge to detect when and where the adsorption region change into the non-adsorption region, and then to interchange the adsorption kinetics. The question is how to simulate such discrete events. This problem is dealt with in the presentation of the following numerical solution methodology.

To replace the LDF model Eq. (2b) with Eq. (10) in the PDAE system, switching functions are used to detect the discrete event (or state change). A generalized rate equation based on the switching functions is proposed for the binary system as follows:

$$\begin{cases} r_A^{general} = \phi_{sum} \cdot \phi_{product} \cdot r_A \\ r_B^{general} = -r_A^{general} \end{cases} \tag{11a}$$

where $r_A \equiv dn_A / dt = k(n_A^* - n_A)$ from Eq. (2b). The sum kernel (ϕ_{sum}) and product kernel ($\phi_{product}$) are defined for a binary system with A and B components:

$$\begin{cases} \phi_{sum} = 0, \; if \;\; C_A + C_B \le 0.0 \\ \phi_{sum} = 1, \; elsewhere \end{cases} \tag{11b}$$

$$\begin{cases} \phi_{product} = 0, \; if \;\; C_A \cdot C_B < 0.0 \\ \phi_{product} = 1, \; elsewhere \end{cases} \tag{11c}$$

This formulation satisfies the electro-neutrality condition in the solid phase (i.e., $\sum_i r_i = 0$), as will be shown in Fig. 7, and is identical to the conventional LDF model, Eq. (2b), in the nonequilibrium zone. It is essential that the switching functions Eq. (11b) and Eq. (11c) are applicable to an explicit time integrator such as the conservation

element and solution element (CE/SE) method[14,17] that is used in this study. An alternative form of the switching function[22] is used for an implicit ODE time integrator such as DASSL[10].

The problem type encountered in this ion-exchange SMB unit belongs to the class of discrete events or a hybrid problem.[28] This problem type is presented by switching between the two kinetic expressions in Eq. (10) and implemented using the so-called generalized rate equation in Eq. (11) for the time-marching CE/SE scheme. This generalized model is considered as a numerical implementation rather than a physical model, which renders the generalized version of the non-equilibrium model (i.e., LDF model) feasible even in equilibrium regions.

3.2 Adsorption isotherms

The equilibrium concentration (or adsorption isotherm) plays an important role in the column model Eq. (2). The adsorption isotherm intrinsically decides separation performance. Remember that the feed solution of the NPK ion-exchanger is a concentrated electrolyte solution with cations (Ca^{2+}, H^+ and K^+) and counterpart anions (NO_3^-, PO_4^{3-} and eventually Cl^-). Due to the strong electrolyte, a nonlinear adsorption isotherm is expected.

An empirical correlation is proposed for the binary adsorption (Ca^{2+}-H^+ and K^+) on Purolite 160C resin as a fifth-order polynomial function fitted to experimental data of a 3.3N solution.

$$n_A^* = n_T x_A (2.2321 - 7.66474 x_A + 17.714 x_A^2 - 18.882 x_A^3 + 7.6032 x_A^4) \quad (12a)$$

$$n_B^* = n_T - n_A^* \quad (12b)$$

where the subscripts A and B denote the Ca^{2+}-H^+ and K^+ component, respectively, n_T is the resin capacity and $x_A = \frac{C_A}{C_A + C_B}$ is the liquid mole fraction of A. Eq. (12b) implies the electro-neutrality condition in the solid phase at equilibrium (i.e., $\sum_i n_i^* = n_T$). Eq. (12) is used over the whole concentration range in this study. All concentrations are based on equivalent mole concentration (eqv/l). Fig. 3 illustrates experimental points and their fitting curve at C_{A+B}=*3.3N*.

A more complex model for NPK concentrated solutions can be developed on the basis of thermodynamic equilibrium constants for which non-ideality in liquid and resin phases is taken into account.[23] Activity coefficients in the solution are calculated by an extended Debye-Hückel expression and those on the resin by the Wilson VLE model under the assumption of an analogy between solute/resin and vapor/liquid system.[24] The thermodynamic equilibrium model predicts equilibrium concentrations of the three cation components (Ca^{2+}-H^+

and K^+) in the concentration range up to 12N within an experimental error that is estimated to be 1-2 % of the total resin capacity.[23]

To find dependency of the equilibrium line upon various liquid concentrations, the equilibrium lines are obtained on the basis of the thermodynamic equilibrium model[23]. Fig. 4 demonstrates that the equilibrium concentration of A (y_A) calculated by the thermodynamic model varies slightly within $3 \le C_{A+B} \le 10\ eqv/l$. Even though the thermodynamic equilibrium model provides more reliable adsorption isotherms over the broad concentration range, Eq. (12) is used in this study because i) simulation (e.g., model parameter estimation, sensitivity analysis and optimization) with the thermodynamic equilibrium model requires much longer computational time than Eq. (12) because of nonlinear iteration procedures in solving the thermodynamic model, ii) Eq. (12) predicts relatively well over the interesting concentration range, $3.0 \le C_{A+B} \le 8.0\ eqv/l$, as shown in Fig. 4, and iii) there is no significant difference between simulation results with Eq. (12) and those with the thermodynamic equilibrium model as seen in Tables 4 and 5.

4. *In situ* experiments, simulation and optimization results

Mathematical models are desired to represent experimental results as closely as possible. Section 3 presents a relatively simple SMB model. Therefore, the model should be validated by comparing experimental data and simulation results. Once the model is validated and the simulation results are found to agree reasonably with experimental data, it can be used for model-based optimization of operating conditions.

In this section, simulation results and *in situ* experiments are compared both for the pilot- and industrial-scale plants. Due to uncertainty of the model parameters such as resin capacity, bed voidage, dispersion coefficient, mass transfer coefficient and adsorption isotherm, then sensitivity analysis is performed for these parameters. Experimental and simulation procedures are presented in the following sub-section.

4.1 Experimental and simulation procedures

The total of 16 tests were carried out by experienced staff at the industrial company on the pilot plant configured as [2/5/2-1-1/4/1]. The tests were performed within the feasible operating region, changing the shifting time (or cycle time) and the two flowrates (V1 and FS). The 16 tests are composed of four different flowrates of V1 at three different cycle times (5, 6, and 7 min) and four different flowrates of FS at the 5-min cycle time, as shown in Table 3. Table 1 shows experimental conditions for one of the 16 tests (test # P3 in Table 3). Only one test was performed in the industrial-scale plant configured by [3/3/3-1-1/4/1] as reported in Table 2.

The feed compositions of TS and TK changed a little according to feed preparation, as shown in Tables 1 and 2. However, their fluctuations are small. During the cycle time, V1, V2, TS and TK were injected with a constant flowrate and at the same time FS, KK and SV were withdrawn also at a constant flowrate. KV was recycled to V1. The fresh V1 flowrate was (V1-KV) due to the recycle flow.

Before carrying out each test, all the columns were washed out and filled with fresh water. To reach a pseudo cyclic steady-state, 3 rounds (48 shiftings) were operated under the same conditions. After the pre-loading, 1 round (16 shiftings) was performed for the data analysis. Thus, total 4 rounds (about 5 hours) were run for each test. Each solution withdrawn at each shifting in the 4th round was collected in four tanks for each of FS, KK, SV and KV. The four solutions were subsequently analyzed in the laboratory. As a result, the analyzed concentrations were average values over the last round.

For the key components (A for Ca^{2+}-H^+ and B for K^+), the purity and the dilution are determined from laboratory analysis:

$$purity = \frac{\overline{C}_{B\ or\ A\ in\ FS\ or\ KK}}{\left(\overline{C}_A + \overline{C}_B\right)_{FS\ or\ KK}} \tag{13}$$

$$dilution = 1 - \frac{\left(\overline{C}_A + \overline{C}_B\right)_{FS\ or\ KK}}{\left(\overline{C}_A + \overline{C}_B\right)_{TS\ or\ TK}} \tag{14}$$

where $\overline{C}_A$ *or* $\overline{C}_B$ is the measured average concentration. A high purity of K^+ in the FS solution means a high quality of the product. The purity of $Ca^{2+} - H^+$ in the KK solution indicates how much the $Ca^{2+} - H^+$ ions absorbed on the resin are desorbed in the regeneration section. Thus, the higher the purity becomes in the KK solution, the higher the purity will be in the FS solution. The dilution indicates a loss of all valuable ions such as NPK on ion-form, i.e., NO_3^-, PO_4^{3-} and K^+.

Two samples of resin particles of the regenerated resin (BW column) and the exhausted resin (V1 column) are also analyzed in the laboratory, after finishing a test at the three cycle times (5, 6 and 7 min). Thus, the solid concentration of the resin is also an average value for the two columns.

Simulation is performed for 15 columns, i.e., excluding one backwashing column, during 53 shiftings. The simulation parameters are also shown in Table 1 and Table 2. For the sensitivity analysis of the five model parameters (see Table 7), at least 10 runs should be done. In the simulations, concentration profiles exhibit steep moving fronts in several places, as will be shown in Fig. 6. Thus, a fast and accurate numerical scheme is desirable to solve the SMB model Eq. (2)-(5).[14] The non-iterative space-time CE/SE method[14,25] is used for solving the conservation laws represented by partial differential equations in Eq. (2) for each column.

At the beginning of the first shifting (i.e., t=0), the liquid concentration of all components is initialized to zero for all columns. The resin is initially set to 75% K^+-form and 25% Ca^{2+}/H^+-form for all columns:

$$C_A(0, z_{i,k}) = C_B(0, z_{i,k}) = 0, \; for \; i = 1 \cdots N_m, \; k = 1 \cdots 15 \tag{15a}$$

$$n_A(0, z_{i,k}) = 0.25 n_T, \; n_B(0, z_{i,k}) = 0.75 n_T, \; for \; i = 1 \cdots N_m, \; k = 1 \cdots 15 \tag{15b}$$

where N_m is the number of meshes per column and n_T is the resin capacity. The assumption Eq. (15b) is somewhat unrealistic, because the initial resin concentration profile depends on the previous run and is not uniform (see Fig. 7). Eq. (15b) is however adopted because of the lack of information on the initial resin concentration. The effect of the unrealistic initial condition is negligible after 2 rounds of simulation. Each run is completed after 53 shiftings (3.5 rounds for 15 columns).

All simulations are performed on a PC equipped with a single 1.3GHz processor. The number of mesh points per column is given to $N_m=26$ for all the cases and the number of time steps per cycle time is $N_t=71$. As a result, the CFL number $\nu \equiv v_L \frac{\Delta t}{\Delta z} \approx 0.6$, where $\Delta t = \frac{\tau}{(N_t - 1)}$ and $\Delta z = \frac{L_{c,eff}}{(N_m - 1)}$. The computational time is less than 1 minute for each run. It is expected that the effects of the number of mesh points and the CFL number are not significant, because for the NPK fertilizer process the Peclet number is not large, $Pe = 65 \sim 105$ and the Stanton number is small, $St = 1.4 \sim 5.7$ (see Table 1 and Table 2).[14]

In the simulation, the average liquid concentrations in the FS and KK solutions are obtained from the numerical integration[30] of liquid concentrations at the exit of FS and KK columns over the last shifting (i.e., 53rd shifting):

$$\overline{C}_{k,53^{rd}\ shifting} = \frac{\sum_{i=1}^{N_t} C_{k,i} \Delta t}{\tau}, \; k=A \; or \; B \tag{16}$$

where N_t is the number of time steps. The average resin concentrations are also based on the values at the end of the last shifting. The 10th column and the first column are used for the regenerated resin (BW column in the experiment) and the exhausted resin (V1 column in the experiment) analyses, respectively. The average resin concentrations for each component are obtained as follows.

$$\overline{n}_{k,53^{rd}\ shifting} = \frac{\sum_{i=1}^{N_m} n_{k,i} \Delta z}{L_{c,\,eff}}, \; k=A \; or \; B \tag{17}$$

In Tables 4 and 5, the two average concentrations ($\overline{C}$ *and* $\overline{n}$) obtained from experiments and simulations are reported for the industrial-scale plant. The model parameters mentioned in section 3 were estimated and

confirmed on the basis of the 16 pilot-plant experiments, which is essential for model-based simulation and optimization.

4.2 Pilot-plant results

Simulation results performed at the operating conditions shown in Table 1 are illustrated in Lim and Lee (2007)[19]. The maximum deviation between simulation and experiment remains within about 10% in absolute deviation for the purity of 16 pilot-plant experiments. The trends of the purity variations also exhibit good agreement for all the cycle times.[19]

It is important to notice that this 6-zone SMB process is operated at a relatively low purity (60-70%, see Table 4) of the product solution, since the amount of valuable NO_3^- and PO_4^{3-} in the dilution stream also increase when the process is operated at a higher potassium purity.

In Fig. 5, the operating conditions of the 16 experimental tests are plotted in the space of m_2-m_5, where m_2 is the zone II fluid to solid flowrate ratio ($m_2 = \frac{Q_2}{Q_s}$) and m_5 is the zone V fluid to solid flowrate ratio ($m_5 = \frac{Q_5}{Q_s}$). Here, the most important zones (zone II and zone V) in this two-section SMB process are analyzed within the m-plane (i.e., fluid-solid flowrate ratio plane) like Triangle theory[26] developed on the basis of equilibrium adsorption, linear or Langmuir isotherms for the TMB operation. The tests #1-4, #5-8 and #9-12 are performed by changing m_2 at a constant m_5. Purity shows a tendency to decrease as operation moves away from the diagonal line in Fig. 5.[19] The tests #13-16 are carried out with constant m_2 and m_5. The above reported experimental and calculated purity trends are compatible with Triangle theory. However, the separation performance measures (purity, productivity and desorbent consumption) of this SMB unit are not straightforwardly optimized by the Triangle theory, since adsorption isotherms are strongly nonlinear and the process is operated in a non-traditional way. This will be further explored below after discussing results from the industrial plant.

4.3 Industrial plant results

One experiment is carried out in the industrial plant at the experimental (and simulation) conditions given in Table 2. It is observed that the experimental average liquid concentrations ($\overline{C}_j$) during the whole 4th-round (i.e., from 46 to 60 shiftings) are in good agreement with the simulation results within a 3% error bound (see Table 4).

Table 4 reports average concentrations, purity and dilution in the FS and KK solutions at the final shifting. To investigate effects of the adsorption isotherm model on the process performance, two simulations with the two-

component model in Eq. (12) and with the three-component model[23] are performed. The two simulation results are in good agreement, as shown in Tables 4 and 5. Table 5 summarizes the *in situ* experimental and simulation results of solid concentrations in the BW column (or regenerated resin) and V1 column (or exhausted resin). Some differences between experiments and simulations are observed in the average resin concentrations. However, the resin utility of the simulation agrees well with that of the experiment. In Table 4 and Table 5, it is demonstrated that the polynomial adsorption isotherms Eq. (12) fitted to experimental points represent the rigorous 3-component model[23] well. Note in Tables 4-5 that the concentrations of component A which are obtained from the three component-based thermodynamic model[23] are the sum of those of the two components, Ca^{2+} and H^{+}.

For the final shifting (53rd shifting), liquid and solid concentrations of Ca^{2+}-H^{+} and K^{+} are illustrated along the column number in Fig. 6 and Fig. 7, respectively, at 3 different times during the 5 min cycle. At the beginning of the cycle (t=0), TS and TK are fed at z=3 and z=10, respectively, while FS and KK start to be withdrawn at z=6 and z=14, respectively. The four positions (z=3, 6, 10 and 14) are depicted as the dashed lines in Fig. 6 and Fig. 7. Total concentrations at each axial position are shown in the bold dotted line. Slight overshoots caused by the feed is observed at the feed points (z=3 and z=10) in Fig. 6 (a). Discontinuous concentrations at z=2 and z=9 (inlet points of the 3rd column and 10th column) in Fig. 6 (a) originate from the concentrations at the feed points (z=3 and z=10) of the previous cycle. The Ca^{2+}-H^{+} concentration at the FS port (z=6) is effectively zero and the K^{+} concentration is low (i.e., high purity and low concentration of K^{+}) due to the one-column advanced operation.

At the middle of the cycle in Fig. 6 (b), a maximum point of the K^{+} concentration is reached at z=6 and that of the Ca^{2+}-H^{+} at z=14. Fig. 6 (c) shows concentration profiles at the end of the cycle (t=5 min). These dynamic behaviors during one cycle represent the cyclic stationary state which is repeated over the next cycle. Note that the concentration dynamics shown in Fig. 6 and 11 cannot be obtained from TMB[3-4] or CMB[5-6] models. Indeed, the TMB or CMB models provide just one steady state concentration profile along the columns. For nonlinear adsorption isotherms, the profile of the TMB models can be quite different from that of the SMB models at the middle of the cycle time, which demonstrates that SMB processes have to be described by rigorous dynamic models such as the SMB model Eq. (2)-(5).[27]

The cyclic stationary state is shown for resin concentration distributions over the columns in Fig. 7. Owing to the counter-current-like flow of the SMB operation, the regenerated resin passing the 7th column ($6 \le z \le 7$) contacts with the reactive solution at the 6th column ($5 \le z \le 6$). The exhausted resin is found at the first column ($0 \le z \le 1$). The resin concentration profiles give important information on the resin performance and design, since the process performance is directly related to resin utility in Fig. 8. The total liquid concentration is constant globally over the

production zone II (3≤z≤6) and the regeneration zone V (10≤z≤14) in Fig. 6 (b). The total concentration in the solid phase is equal to the resin capacity everywhere in Fig. 7. Thus the electro-neutrality condition in Eq. (11a) and Eq. (12) is satisfied both in the liquid and the solid phases.

It is worth noting that inactive regions (or non-adsorption regions because of equilibrium, $(C_A + C_B) \approx 0$) are found in many places (see Fig. 6) where the resin is saturated with $Ca^{2+} - H^+ - K^+$ ions (see Fig. 7). The equilibrium correlation Eq. (12a) is valid only for $(C_A + C_B) \neq 0$. If Eq. (2) is used for all regions instead of Eq. (10) or Eq. (11), a virtual desorption could take place in these inactive regions to satisfy the electro-neutrality condition, as mentioned in Section 3.4. Therefore, unphysical numerical results (e.g., negative concentrations) can be obtained by employing the traditional LDF model Eq. (2b). Besides, Eq. (12) is infeasible if negative concentrations appear. As a result, it is necessary to use the generalized LDF model Eq. (12) for this ion-exclusion and ion-exchange chromatographic system. This generalized LDF model implies the thermodynamic insight that there is no apparent adsorption/desorption flux, when $(C_A + C_B) = 0$, due to equilibrium between the liquid and solid phases.

The industrial-scale plant with these operating conditions seems not to be fully exploited, because there are too long inactive regions, e.g., zone I (0≤z≤1) and zone III (7≤z≤9), as shown in Fig. 6. It is therefore relevant to investigate the potential benefit from optimizing the operating conditions. Such a study on the industrial-scale process is presented below.

4.4 Optimization results for industrial-scale process

Model-based optimization is performed for the industrial-scale six-zone SMB process (see Table 2). The objective of the optimization problem is to minimize wash-water consumption, while keeping maximum productivity at the given purity level. An optimization procedure (MLOP; multi-level optimization procedure) for this objective is presented in Lim (2004)[29]. The four level optimization approach of MLOP may be briefly summarized as follows:

- Level 1: initialization based on standing wave analysis[5] under the assumption of linear adsorption isotherms.
- Level 2: TMB optimization using nonlinear adsorption isotherms and non-equilibrium design.
- Level 3: SMB optimization for maximization of productivity.
- Level 4: SMB optimization for minimization of desorbent consumption.
- If the procedure has converged close to a constant cycle time, it is terminated else go to level 3.

Since the operating conditions shown in Table 2 are well adjusted through a company procedure , the optimization with MLOP (multi-level optimization procedure)[29] starts at level 3. The optimization variables are the six flowrates (Q_{V1}, Q_{TS}, Q_{FS}, Q_{V2}, Q_{TK} *and* Q_{KK}) and the cycle time (τ). Since Q_{V1} includes the recycle flowrate (Q_{KV}), the net wash-water flowrate at z=0 is assigned as follows:

$$Q_{V1_{net}} = Q_{V1} - Q_{KV} \tag{18}$$

In the optimization problems, Q_{V1} is replaced by the new variable $Q_{V1_{net}}$. The objective function and the constraints at level 3 are specified:

$$\underset{x}{Max}\left[\Pr od = \frac{Q_{FS}\overline{C}_{FS,B}}{N_c \times (1-\varepsilon_b)\times V_c}\right],\ x = Q_{TS}, Q_{FS}, Q_{TK}\ \ and\ \ Q_{KK} \tag{19}$$

subject to

$$0.65 \le y_1 = Pur_{FS,B} \le 1.0 \tag{20a}$$

$$0.85 \le y_2 = Pur_{KK,A} \le 1.0 \tag{20b}$$

$$y_3 = Dilut_{FS} \le 0.45 \tag{20c}$$

$$y_4 = Dilut_{KK} \le 0.55 \tag{20d}$$

$$y_5 = Q_{max} \le 1.75 \tag{20e}$$

where

$$\overline{C}_{FS,B} = \frac{\sum_{i=1}^{N_t} C_{B,i}\Delta t}{\tau}\ \text{ at }\ N_{shift} = 53 \tag{21a}$$

$$Pur_{FS,B} = \frac{\overline{C}_{B\ in\ FS}}{\left(\overline{C}_A + \overline{C}_B\right)_{FS}} \tag{21b}$$

$$Pur_{KK,A} = \frac{\overline{C}_{A\ in\ KK}}{\left(\overline{C}_A + \overline{C}_B\right)_{KK}} \tag{21c}$$

$$Dilut_{FS} = 1 - \frac{\left(\overline{C}_A + \overline{C}_B\right)_{FS}}{\left(\overline{C}_A + \overline{C}_B\right)_{TS}} \tag{21d}$$

$$Dilut_{KK} = 1 - \frac{\left(\overline{C}_A + \overline{C}_B\right)_{KK}}{\left(\overline{C}_A + \overline{C}_B\right)_{TK}} \tag{21e}$$

In Eq. (21a), $\overline{C}_{FS,B}$ is the average concentration of B during the final shifting $N_{shift} = 53$. In Eqs (21d) and (21e), the dilution indicates a loss of all valuable ions such as NPK in the ion-form, i.e., NO_3^- , PO_4^{3-} and K^+ , as stated

above. Note that the process is operated at relatively low purity to reduce loss of NO_3^-, PO_4^{3-} and K^+, as mentioned earlier. The two wash-water flowrates ($Q_{VI_{net}}$ *and* Q_{V2}) and the cycle time (τ) are kept constant at this level.

The objective function and the constraints at level 4 are given:

$$\underset{x}{Min}\left[Q_{des} = Q_{VI_{net}} + Q_{V2}\right],\ x = Q_{VI_{net}}, Q_{V2}, \tau \tag{22}$$

subject to

$$0.65 \le y_1 = Pur_{FS,B} \le 1.0 \tag{23a}$$

$$0.85 \le y_2 = Pur_{KK,A} \le 1.0 \tag{23b}$$

$$y_3 = Dilut_{FS} \le 0.45 \tag{23c}$$

$$y_4 = Dilut_{KK} \le 0.55 \tag{23d}$$

$$y_5 = Q_{max} \le 1.75 \tag{23e}$$

$$29.1 \le y_6 = Prod \tag{23f}$$

where productivity in the production section ($Prod$) is defined as follows:

$$Prod = \frac{Q_{FS}\overline{C}_{FS,B}}{N_c \times (1-\varepsilon_b) \times V_c} \tag{24}$$

Note that the minimum value of productivity in Eq. (23f) is obtained from the optimization results of level 3.

Table 6 reports results of MLOP for the NPK ion-exchange SMB process. Operating conditions and simulation results corresponding to levels 1-2 are referred to Tables 2 and 4. Levels 3 and 4 are repeated once to ensure a converged optimum solution. The values of m_2 and m_5 at each level are also shown in Table 6.

At level 3 and level 3 repeated, higher productivities are achieved by increasing Q_{TS} and Q_{FS}, and by increasing Q_{TK}, decreasing Q_{KK} and increasing Q_{KV} (or recycle flowrate). Since Q_{FS} should increase to augment the productivity in Eq. (24), Q_{TS} and Q_{FS} increase. As shown in the plane m_2-m_5 (see Fig. 5), m_5 decreases at a similar m_2 value (m_2=1.35) to increase productivity. Decreasing m_5 amounts to increase the residence time in the regeneration section, which leads to a higher regeneration ratio of the resin (see also Fig. 8-9).

At level 4 and level 4 repeated, the desorbent consumption is reduced by adjusting the cycle time, while the productivity is maintained. In this case, m_2 increases at a similar m_5 value (m_5=1.52) to decrease wash-water consumption (see Fig. 5). Increasing m_2 amounts to decrease the residence time in the production section. Nevertheless, productivity remains high by keeping a high regeneration ratio of the resin (see Table 6).

The optimization result is that wash-water consumption is reduced by 5.4% ($Q_{des} = 1.454 \rightarrow 1.375$) at a 5% higher productivity ($Prod = 28.23 \rightarrow 29.65$), compared to the normal operating condition at levels 1-2.

Fig. 8 and Fig. 9 compare concentration distributions over the columns in the liquid and solid phases, respectively. The thin lines indicate component A ($Ca^{2+} + H^{+}$) and the bold lines component B (K^{+}). Concentration profiles are shown at three different times within the 53rd shifting period, i.e., at the beginning (t=0), the middle (t=2/τ) and the end (t=τ) of the 53rd cycle.

Fig. 8 shows that the concentration profiles of A and B are lowered in the production section, while those of A and B are raised in the regeneration section. In Fig. 9, the resin is regenerated much more by K^{+} (or B) at the optimized flowrates and cycle time than at the normal operating condition. This regenerated resin results in a high driving force in the production section, higher productivity and lower desorbent consumption.

4.5 Sensitivity analysis of model parameters

The sensitivity analysis is presented only for the industrial-scale plant. Table 7 shows nominal values and perturbations of the five model parameters: resin capacity (n_T), effective bed voidage ($\varepsilon_{b,eff}$), mass transfer coefficients in the production section (k_{prod}) and in the regeneration section (k_{regen}) and axial dispersion coefficient (D_{ax}).

The resin capacity and the effective bed voidage were determined through experiments by the industrial collaborator. Thus, their perturbations can be considered as potential extreme experimental errors. The mass transfer coefficients and the axial dispersion coefficient were initialized from empirical correlations, as explained in section 3, and were identified through comparing simulation results and experimental data from the pilot plant. Since the effect of D_{ax} / v_L on the process performance is small, a large perturbation (±1000 %) is employed.

Sensitivity ($\frac{dy}{dx}$) of the process performance (y) has the unit according to model parameters (x). However, elasticity ($\frac{dy}{dx} \cdot \frac{x}{y}$) is dimensionless and therefore it is most useful to reveal which parameters most strongly influences the process performance. Table 7 reports sensitivity and elasticity of purity and dilution in the FS solution as well as resin utility according to the five model parameters, where elasticity is shown in parenthesis. The resin capacity (n_T) and the bed voidage ($\varepsilon_{b,eff}$) affect the purity and the resin utility relatively strongly as indicated by their elasticity. As a result, n_T and $\varepsilon_{b,eff}$ should be accurately measured by experiments.

Fig. 10 depicts variations of the purity and the resin utility with respect to four model parameters. Experimental data are marked in filled circles and squares. Note that purity depends positively on the resin capacity (n_T), since a higher n_T implies a higher driving force. However, the resin utility is reduced as n_T increases. In contrast, these relationships are reversed for the bed voidage (see Fig. 10 (a) and (b)). As $\varepsilon_{b,eff}$ increases, the interstitial fluid velocity (v_L) decreases and the ratio of the resin volume to the fluid volume (i.e., $\frac{1-\varepsilon_{b,eff}}{\varepsilon_{b,eff}}$ in Eq. (2a)) also decreases. The former relation results in increasing the resin utility due to the increase of the fluid residence time, while the latter relationship decreases the purity because of a reduced resin volume.

A high mass transfer coefficient means a high adsorption or desorption rate. Therefore, the purity and the resin utility increase, as k_{prod} and k_{regen} increase, where the effect of k_{prod} is about twice that of k_{regen} on the purity and the resin utility (see elasticity in parenthesis in Table 7). These elasticities show that a 10% change of the mass transfer coefficient of the production section (k_{prod}) results in 1.1 % change of FS purity while a 10% change of the mass transfer coefficient of the regeneration section (k_{regen}) results in 0.5 % change of FS purity.

A low axial dispersion coefficient enhances the process performance on purity and resin utility, even though the static effect is small. All of the five model parameters have little effects on the dilution in the FS solution, since the dilution is defined as a loss of total ions in Eq. (14).

Through this sensitivity analysis, the effects of model parameters on the process performance are identified and it is demonstrated that the process performance can be enhanced by adjusting operational conditions to achieve higher k and lower D_{ax}.

5. Conclusions

To perform one experimental test of the NPK ion-exchange SMB process, about 5 hours are required to reach a cyclic stationary state. In order to find optimum operation conditions for the cycle time and flowrates in a given column configuration, many experimental runs must be carried out. Thus, it may take several months to find near optimum operation conditions through experiments.

The non-equilibrium SMB chromatographic model used is characterized by a spatially distributed dynamic system for a number of columns. An explicit time-marching scheme, i.e., the so-called conservation element and solution element (CE/SE) method, is employed to accurately and effectively solve the distributed model described by partial differential equations. The CE/SE method enables accurate and efficient tracking of steep concentration

profiles moving along the column axis. Thereby, simulation, parameter estimation and optimization studies can be accelerated. When using conventional linear driving force (LDF) models for non-equilibrium adsorption, an unphysical desorption can occur in non-adsorption (or inactive) regions of the column where an equilibrium state between the liquid and solid phases may exist. The inactive regions appear during operation for the ion-exchange SMB process due to the wash-water zones which are included to ensure ion-exclusion. A generalized LDF adsorption rate model is used to enable switching between equilibrium and non-equilibrium adsorption models. It is demonstrated that the switching functions enables satisfying the electro-neutrality condition in ion-exchange chromatography.

In the simulation study on the six-zone SMB process, less than one minute is needed to obtain the cyclic stationary state, i.e., about 1/300 of the experimental time, using the CE/SE method. Model parameters (e.g., mass transfer coefficients in production and regeneration sections) are estimated by comparing simulation results with the experimental data. The effects of the model parameters on the process performance are examined through sensitivity analysis. The obtained model results compare favorably both to pilot- and industrial-scale data.

Applying MLOP (multi-level optimization procedure) to NPK ion-exchange SMB chromatography, it is shown that wash-water consumption can be reduced, while also achieving a higher productivity. It is also observed that desorbent consumption can be reduced near the same productivity value adjusting the shifting time thereby also reducing the energy consumption in downstream evaporators.

Acknowledgements

This research was financially supported by the Danish Energy Authority through the grants ENS 1223/99-0008 and ENS 1273/00-0026. The authors appreciate the advice from Dr. Sin-Chung Chang on the application of the space-time CE/SE method to the packed-bed chromatographic model. Thanks go to the innovation department of Kemira Denmark A/S for helpful discussion and providing experimental data.

This work is also financially supported by the Korea Research Foundation (KRF) grant funded by the Korean Government (MOEHRD) through the project number of KRF-2005-D00108.

Nomenclature

AE = algebraic equation

BC = boundary condition

C = concentration in fluid phase (eqv/l on liquid volume basis)

$\overline{C}$ = average liquid concentration (eqv/l on liquid volume basis)

C_{in} = inlet concentration of fluid at z=0 (eqv/l on liquid volume basis)

CE/SE = conservation element/solution element

CMB = continuous moving bed

DAE = differential algebraic equation

D_{ax} = axial dispersion coefficient (m^2/min)

D_c= column inner diameter (m)

$g(C)$ = adsorption isotherm function in Eq. (2c)

IC = initial condition

k = overall adsorption rate coefficient (1/min)

k_f = liquid film mass transfer coefficient (m/min)

k_{prod} = mass transfer coefficient in the production section (m/min)

k_{regen} = mass transfer coefficient in the regeneration section (m/min)

L_c = column length (m)

$L_{c,eff}$ = effective column length (m)

LDF = linear driving force

m_2= zone II fluid to solid flowrate ratio ($m_2 = Q_2 / Q_s$)

m_5= zone V fluid to solid flowrate ratio ($m_5 = Q_5 / Q_s$)

n = concentration in resin or solid phase (eqv/l on particle volume basis)

n^* = equilibrium concentration in resin or solid phase (eqv/l on particle volume basis)

$\overline{n}$ = average solid concentration (eqv/l on particle volume basis)

N_m = number of mesh points per column

NPK = nitrogen-phosphate-potassium

N_{shift} = number of shiftings

n_T = resin capacity (eqv/l on bed volume basis)

$n_{T,p}$ = resin capacity (eqv/l on particle volume basis)

N_t = number of time steps per cycle time

ODE = ordinary differential equation

PDAE = partial differential algebraic equation

PDE = partial differential equation

Pe = Peclet number (=$v_L L_{c,eff}/D_{ax}$ or $v_L d_p/D_L$)

Q = flowrates (m^3/min)

Q_2 = flowrate of zone II (m^3/min)

Q_5 = flowrate of zone V (m^3/min)

Q_{in} = inlet flowrate of fluid at z=0 (m^3/min)

Q_s = flowrate of solid particles, $Q_s = (1-\varepsilon_{b,eff}) \cdot A_c \cdot L_{c,eff} / \tau$ (m^3/min)

r_i = adsorption rate (eqv/l/min)

$r_i^{general}$ = generalized adsorption rate (eqv/l/min)

S = cross-section area of column (m^2)

SMB = simulated moving bed

St = Stanton number (=$kL_{c,eff}/v_L$)

t = time (min)

T = temperature (^oC)

TMB = true moving bed

V_{dead}: dead volume (m^3)

v_L = interstitial fluid velocity (m/min)

V_{liquid}: liquid volume (m^3)

V_{total}: sum of dead volume and liquid volume (m^3)

x_A = mole fraction of $C_{Ca^{2+}-H^+}$ to total liquid concentration

y_A = mole fraction of $n^*_{Ca^{2+}-H^+}$ to total solid concentration

z = axial direction of column (m)

Greek letters

α = logical variables in the node model, Eq. (5)

ε_b = interstitial bed voidage

$\varepsilon_{b,eff}$ = effective interstitial bed voidage

ϕ_{sum} = sum kernel in Eq. (11)

$\phi_{product}$ = product kernel in Eq. (11)

ν = CFL number

τ = cycle time or shifting time

Δt = uniform time step size (=min)

Δz = uniform spatial step size (=m)

Reference

(1) Klatt, K.-U.; Dunnebier, G.; Hanisch, F.; Engell, S. Optimal operation and control of simulated moving bed chromatography: A model-based approach. AIChE symposium series 326, **2002**, 98, 239.

(2) Proll, T.; Kusters, E. Optimization strategy for simulated moving bed systems. J. Chromatogr. A, **1998**, 800, 135.

(3) Ching, C. B.; Chu, K. H.; Hidajat, K.; Uddin, M. S. Experimental and modeling studies on the transient behavior of a simulated countercurrent adsorber, J. Chem. Eng. Jap. **1991**, 24(5), 614.

(4) Beste, Y. A.; Lisso, M.; Wozny, G.; Arlt, W. Optimization of simulated moving bed plants with low efficient stationary phases: separation of fructose and glucose. J. Chromatogr. A. **2000**, 868, 169.

(5) Ma, Z; Wang, N.-H. L. Standing wave analysis of SMB chromatography: Linear systems, AIChE J., **1997**, 40(10), 2488.

(6) Xie, Y.; Wu, D.; Ma, Z.; Wang, N.-H. L. Extended standing wave design method for simulated moving bed chromatography: linear systems. Ind. Eng. Chem. Res. **2000**, 39, 1993.

(7) Ruthven, D. M.; Ching, C. B. Counter-current and simulated counter-current adsorption separation processes. Chem. Eng. Sci. **1989**, 44(5), 1011.

(8) Juke, A.; Epping, A.; Schmidt-Traub, H. Optimal design of batch and simulated moving bed chromatographic separation processes. J. Chromatogr. A. **2002**, 944, 93.

(9) Wooley, R; Ma, Z.; Wang, N.-H. L. A nine-zone simulated moving bed for the recovery of glucose and xlyose from biomass hydrolyzate. Ind. Eng. Chem. Res. **1998**, 37, 3699.

(10) Petzold, L. R. DASSL, a software package for the solution of differential/algebraic systems of equations. Sandia National Laboratories, Livermore, CA, **1991**.

(11) Melis, S.; Markos, J.; Cao, G.; Morbidelli, M. Separation between amino acids and inorganic ions through ion exchange: Development of a lumped model. Ind. Eng. Chem. Res. **1996**, **35**, 3629.

(12) Dunnebier, G.; Weirich, I.; Klatt, K.-U. Computationally efficient dynamic modeling and simulation of simulated moving bed chromatographic processes with linear isotherms. Chem. Eng. Sci. **1998**, 53(14), 2537.

(13) Lim, Y. I.; Le Lann, J. M.; Joulia , X. Accuracy, temporal performance and stability comparisons of discretization methods for the solution of Partial Differential Equations (PDEs) in the presence of steep moving fronts. Comp. Chem. Eng. **2001**, 25, 1483.

(14) Lim, Y. I.; Jørgensen, S. B., A fast and accurate numerical method for solving simulated moving bed (SMB) chromatographic separation problems. Chem. Eng. Sci. **2004**, 59(10), 1931.

(15) Chang, S. C. The method of space–time conservation element and solution element-A new approach for solving the Navier–Stokes and Euler equations. J. Comput. Phys. **1995**, 119, 295.

(16) Chang, S. C. Courant number insensitive CE/SE schemes. In 38th AIAA joint propulsion conference, AIAA-2002-3890, Indianapolis, USA, **2002**.

(17) Lim, Y. I.; Chang, C. S.; Jørgensen, S. B. A novel partial differential algebraic equation (PDAE) solver: iterative conservation element/solution element (CE/SE) method. Comput. Chem. Eng. **2004**, 28(8), 1309.

(18) Knudsen, K.C. The production of NPK fertilizers by ion-exchange. J. Appl. Chem. Biotechnol. **1974**, 24, 701.

(19) Lim, Y.-I. Lee, A. L. Simulation of a six-zone simulated moving bed chromatographic process for NPK fertilizer production, Kor. Che. Eng. Res. **2007**, 45 (1), in press.

(20) Migliorini, C.; Mazzotti, M.; Morbidelli, M. Simulated moving bed units with extra-column dead volume. AIChE J. **1999**, 45(7), 1411.

(21) Mackenzie, J. A.; Robertson, M. L. The numerical solution of one-dimensional phase change problems using an adaptive moving mesh method. J. Comput. Phys. **2000**, 161(2), 537.

(22) Lim, Y. I.; Christensen, S.; Jørgensen, S. B. A generalized adsorption rate model based on the limiting-component constraint in SMB chromatographic separation. In European Symposium on Computer-Aided Chemical Engineering 13; Kraslawski, A., Turunen, I., Eds.; Elsevier Science B.V.: Amsterdam, 2003; p 767.

(23) Marcussen, L. Multicomponent adsorption of ions from concentrated solutions. Superfos-DTU internal report; Dept. Chem. Eng.: DTU, Denmark, 1985.

(24) Smith, R. P.; Woodburn, E. T. Prediction of multicomponent ion exchange equilibria for the ternary system SO_4^{2-}-NO_3^--Cl^- form data of binary systems. AIChE. J. **1978**, 24(4), 577.

(25) Molls, T.; Molls, F. Space-time conservation method applied to Saint Venant equations. J. Hydraulic Eng. **1998**, 124(5), 501.

(26) Mazzotti, M.; Storti, G.; Morbidelli, M. Optimal operation of simulated moving bed units for nonlinear chromatographic separations. J. Chromatogr. A. **1997**, 769, 3.

(27) Strube, J.; Altenhoner, U.; Meurer, M.; Schmidt-Traub, H.; Schulte, M. Dynamic simulation of simulated moving-bed chromatographic processes for the optimization of chiral separations. J. Chromatogr. A. **1997**, 769, 81.

(28) Mao, G.; Petzold, L.R. Efficient integration over discontinuities for differential-algebraic systems. Computers and Mathematics with applications, **2002**, 43, 65.

(29) Lim, Y. I. An optimization strategy for nonlinear simulated moving bed chromatography: multi-level optimization procedure (MLOP). Kor. J. Che. Eng. **2004**, 21(4), 836.

(30) Storti, G.; Masi, M.; Paludetto, R.; Morbidelli, M.; Carra, S. Adsorption separation processes: countercurrent and simulated countercurrent operations. Comput. Chem. Eng. **1998**, 12(5), 475.

List of Tables

List of Figures

Table 1. Operating conditions and simulation parameters for the pilot SMB plant (*V1/TS/FS-V2/TK/KK = 10.7/2.1/5.6-11.3/3.8/8.8 l/cycle*).

	Production section			Regeneration section		
	Zone I	Zone II	Zone III	Zone IV	Zone V	Zone VI
Q (l/min)	2.14	2.56	1.44	2.26	3.02	1.26
v_L (m/min)	0.494	0.591	0.332	0.521	0.697	0.291
D_{ax} (m^2/min)	$0.02v_L$	$0.02v_L$	$0.02v_L$	$0.02v_L$	$0.02v_L$	$0.02v_L$
k (min^{-1})	0.40	0.40	0.40	0.70	0.70	0.70
Pe ($L_{c,eff}v_L/D_{ax}$)	105	105	105	105	105	105
St ($L_{c,eff}k/v_L$)	1.71	1.43	2.54	2.83	2.12	5.07
Column information	Length ($L_{c,eff}$, m)	D_c (m)		Bed voidage ($\varepsilon_{b,eff}$)		Column number
	2.107*	0.1		0.5522**		15 (2/5/2-1/4/1)***
Inlet concentration	V1	TS		V2		TK
(C_{in}, eqv/l)	$C_{in,A}= C_{in,B}= 0$	$C_{in,A}$=9.93, $C_{in,B}$=0.01		$C_{in,A}= C_{in,B}= 0$		$C_{in,A}$= 0.11, $C_{in,B}$=3.82
Simulation	Mesh number (N_m)	Shifting time (τ, min)		Shifting number (N_{shift})		Resin capacity ($n_{T,p}$)
parameters	26	5		53		3.17****

* L_c=1.492 m

** ε_b=0.37 and V_{dead}= 4.77 litters

*** one backwashing column is not taken into account.

**** $n_{T,p}(=\frac{n_T}{1-\varepsilon_b})$ has the units [eqv/l] on the basis of the particle volume, where $n_T(=2.0\pm0.1)$ is on the basis of the bed volume.

Table 2. Operating conditions and simulation parameters for the industrial-scale SMB plant (*V1/TS/FS-V2/TK/KK = 4.7/1.17/2.03-5.33/2.20/4.77 m^3/cycle*).

	Production section			Regeneration section		
	Zone I	Zone II	Zone III	Zone IV	Zone V	Zone VI
Q (m^3/min)	0.94	1.174	0.768	1.066	1.506	0.552
v_L (m/min)	0.541	0.676	0.442	0.614	0.868	0.318
D_{ax} (m^2/min)	$0.04v_L$	$0.04v_L$	$0.04v_L$	$0.04v_L$	$0.04v_L$	$0.04v_L$
k (min^{-1})	0.40	0.40	0.40	0.70	0.70	0.70
Pe ($L_{c,eff}v_L/D_{ax}$)	65	65	65	65	65	65
St ($L_{c,eff}k/v_L$)	1.93	1.54	2.36	2.97	2.10	5.73
Column information	Length ($L_{c,eff}$, m)	D_c (m)		Bed voidage ($\varepsilon_{b,eff}$)		Column number
	2.605*	2.0		0.5527**		15 (3/3/3-1/4/1)***
Inlet concentration	V1	TS		V2		TK
(C_{in}, eqv/l)	$C_{in,A}= C_{in,B}= 0$	$C_{in,A}=10.37$, $C_{in,B}=0$		$C_{in,A}= C_{in,B}= 0$		$C_{in,A}=0$, $C_{in,B}=3.884$
Simulation	Mesh number (N_m)	Shifting time (τ, min)		Shifting number (N_{shift})		Resin capacity ($n_{T,p}$)
parameters	26	5		53		3.17****

* L_c=1.85 m

** ε_b=0.37 and V_{dead}= 2.37 m^3

*** one backwashing column is not taken into account.

**** $n_{T,p}(=\frac{n_T}{1-\varepsilon_b})$ has the units [eqv/l] on the basis of the particle volume, where $n_T(=2.0\pm0.1)$ is on the basis of the bed volume.

Table 3 Experimental task matrix in the pilot plant (ref: Kemira A/S internal report).

test #	cycle time, sec	Production section				Regeneration section			
		V1 l/cycle	TS l/cycle	FS l/cycle	SV l/cycle	V2 l/cycle	TK l/cycle	KK l/cycle	KV l/cycle
P1	300	13.0	2.1	5.6	9.5	11.3	3.8	8.8	6.3
P2	300	11.4	2.1	5.6	7.9	11.3	3.8	8.8	6.3
P3	300	10.7	2.1	5.6	7.2	11.3	3.8	8.8	6.3
P4	300	10.0	2.1	5.6	6.5	11.3	3.8	8.8	6.3
P5	360	13.0	2.5	6	9.5	11.3	4.3	8.8	6.8
P6	360	11.4	2.5	6	7.9	11.3	4.3	8.8	6.8
P7	360	10.7	2.5	6	7.2	11.3	4.3	8.8	6.8
P8	360	10.0	2.5	6	6.5	11.3	4.3	8.8	6.8
P9	420	13.0	2.9	6.4	9.5	11.3	4.8	9.3	6.8
P10	420	11.4	2.9	6.4	7.9	11.3	4.8	9.3	6.8
P11	420	10.7	2.9	6.4	7.2	11.3	4.8	9.3	6.8
P12	420	10.0	2.9	6.4	6.5	11.3	4.8	9.3	6.8
P13	300	10.7	2.1	5.1	6.2	11.3	3.8	8.3	6.8
P14	300	10.7	2.1	5.6	6.7	11.3	3.8	8.3	6.8
P15	300	10.7	2.1	6.1	7.2	11.3	3.8	8.3	6.8
P16	300	10.7	2.1	6.6	7.7	11.3	3.8	8.3	6.8

Table 4. *In situ* experimental data and simulation results for average liquid concentrations, purity and dilution in the industrial-scale SMB plant.

	Concentration in FS				Concentration in KK			
	A (eqv/l)	B (eqv/l)	Purity (%)	Dilution (%)	A (eqv/l)	B (eqv/l)	Purity (%)	Dilution (%)
Experimental data	2.23	3.74	62.7	42.2	1.59	0.20	88.8	53.9
Simulation with Eq. (12)	2.23	3.82	63.2	41.8	1.60	0.21	88.3	53.5
Simulation with a thermodynamic equilibrium model	2.21	3.83	63.5	41.8	1.61	0.21	88.6	53.5

Table 5. *In situ* experimental data and simulation results for average resin concentrations and resin utility in the industrial-scale SMB plant.

	Resin of BW column			Resin of V1 column			Resin utility* (%)
	A (eqv/l)	B (eqv/l)	% in K^+-form	A (eqv/l)	B (eqv/l)	% in K^+-form	
Experimental data	0.67	2.46	78.6	2.79	0.37	11.7	66.9
Simulation with Eq. (12)	0.51	2.68	84.0	2.63	0.56	17.6	66.4
Simulation with a thermodynamic equilibrium model	0.43	2.76	86.7	2.57	0.62	19.5	67.2

* Resin utility= (% in K^+-form)$_{BW\ column}$ - (% in K-form)$_{V1\ column}$.

Table 6. Results of the MLOP for the NPK ion-exchange SMB process.

	Variables[1]									Simulation results			Objective
	$Q_{V1_{net}}$	Q_{TS}	Q_{FS}	Q_{V2}	Q_{TK}	Q_{KK}	m_2	m_5	τ (min)	Pur_{FS} (%)	$Prod_{FS}$	Q_{max} [2]	functions
1-2 level	0.388	0.234	0.406	1.066	0.440	0.954	1.30	1.67	5.00	63.2	28.23	1.51	*Prod*=28.23[3] Q_{des}=1.454[4]
3rd level	″ [5]	0.236	0.409	″	0.481	0.944	1.36	1.71	″	65.0	29.19	1.547	*Prod* =29.19

													Q_{des} =1.454
4th level	0.458	0.236	0.409	0.923	0.481	0.944	1.24	1.51	4.87	65.0	29.12	1.40	*Prod* =29.12
													Q_{des} =1.381
3rd level	″	0.239	0.428	″	0.505	0.879	1.34	1.54	″	65.0	29.68	1.43	*Prod* =29.68
repeated													Q_{des} =1.381
4th level:	0.456	″	″	0.919	″	″	1.34	1.54	4.88	65.0	29.64	1.42	*Prod* =29.65
repeated													Q_{des} =1.375

[1] all flowrates has the units [$m^3 \cdot min^{-1}$]

[2] $Q_{\max} = \max\left[(Q_{V1} + Q_{TS}), (Q_{V2} + Q_{TK})\right]$

[3] productivity has the units [$mol \cdot min^{-1} \cdot m^{-3}$] based on the total resin volume ($V_S = (1 - \varepsilon_b) L_c S N_c$)

[4] $Q_{des} = Q_{V1_{net}} + Q_{V2}$

[5] This is the same value as that of the cell just above.

Table 7. Sensitivity and elasticity of model parameters on purity, dilution in the FS solution and resin utility.

		n_T	$\varepsilon_{b,eff}$	k_{prod}	k_{regen}	D_{ax}/v_L
Nominal value		2.0	0.5527	0.4	0.7	0.04
Minimum value		1.9	0.5327	0.38	0.65	0.004
Maximum value		2.1	0.5727	0.42	0.75	0.4
Perturbation (%)		±5.0	±3.6	±5.0	±7.1	±1000
Sensitivity*	Purity in FS	10 (0.32)	-40 (-0.35)	17.5 (0.11)	5 (0.05)	-37.5 (-0.02)
(Elasticity**)	Dilution in FS	0 (0)	0 (0)	0 (0)	0 (0)	2.5 (0.002)
	Resin utility	-25 (-0.75)	98 (0.81)	17 (0.10)	6.2 (0.06)	-56.5 (-0.03)

* sensitivity= $\left.\frac{dy}{dx}\right|_{x=nominal\ value}$, where x is the model parameters and y is the purity, dilution or resin utility.

** elasticity= $\left.\frac{d\ ln\ y}{d\ ln\ x}\right|_{x=nominal\ value} = \left.\frac{dy/y}{dx/x}\right|_{x=nominal\ value}$

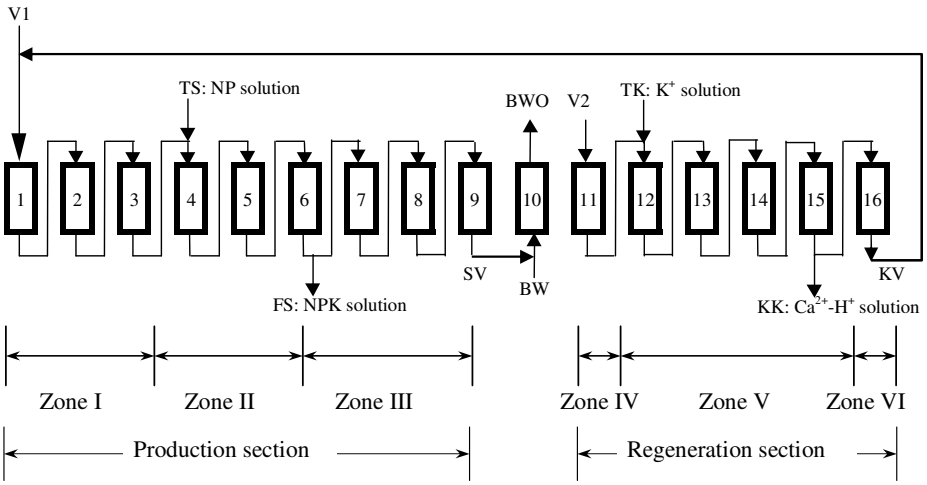

Fig. 1 16 column configuration (3/3/3-1-1/4/1) for a NPK ion-exchange SMB process.

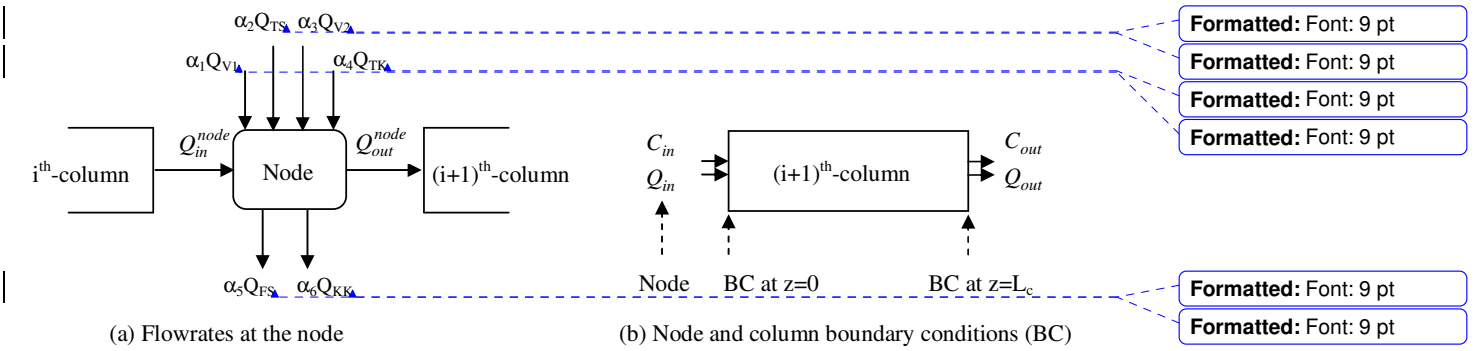

(a) Flowrates at the node (b) Node and column boundary conditions (BC)

Fig. 2. Node and column configurations in this 6-zone SMB process model.

Formatted: Font: 9 pt
Formatted: Font: 9 pt
Formatted: Font: 9 pt
Formatted: Font: 9 pt
Formatted: Font: 9 pt
Formatted: Font: 9 pt

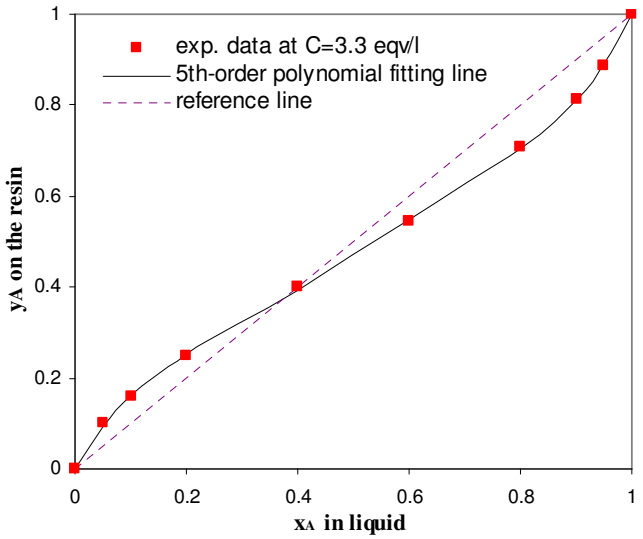

Fig. 3 Experimental points and their fitting curve at *C=3.3 eqv/l*, where $C = C_A + C_B$ and $y_A = n_A^* / n_T$.

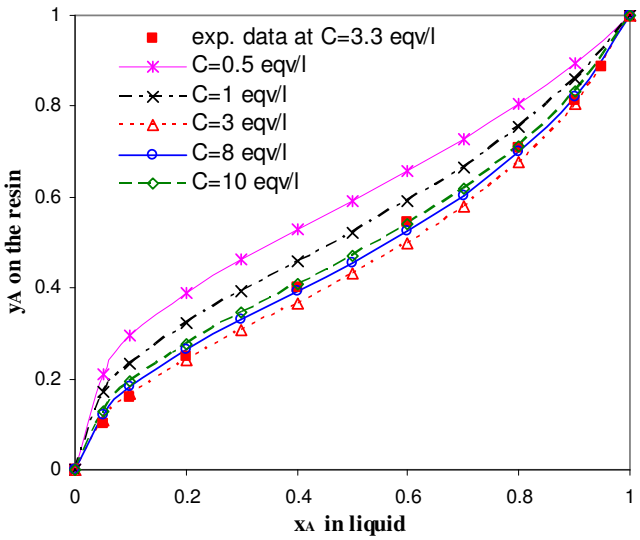

Fig. 4. Equilibrium curves based on a thermodynamic equilibrium model according to total liquid concentration (C), where $C = C_A + C_B$ and $y_A = n_A^* / n_T$.

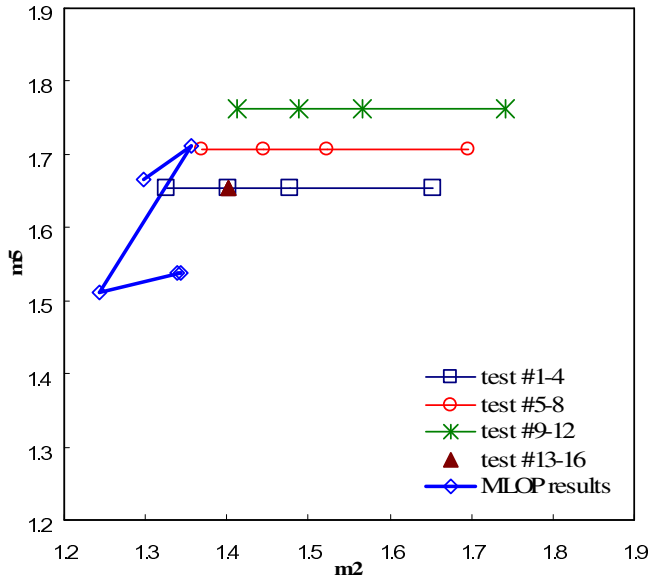

Fig. 5 Flowrate ratio analysis of II and V zones for 16 experimental tests in pilot plant and model-based optimization results in industrial plant.

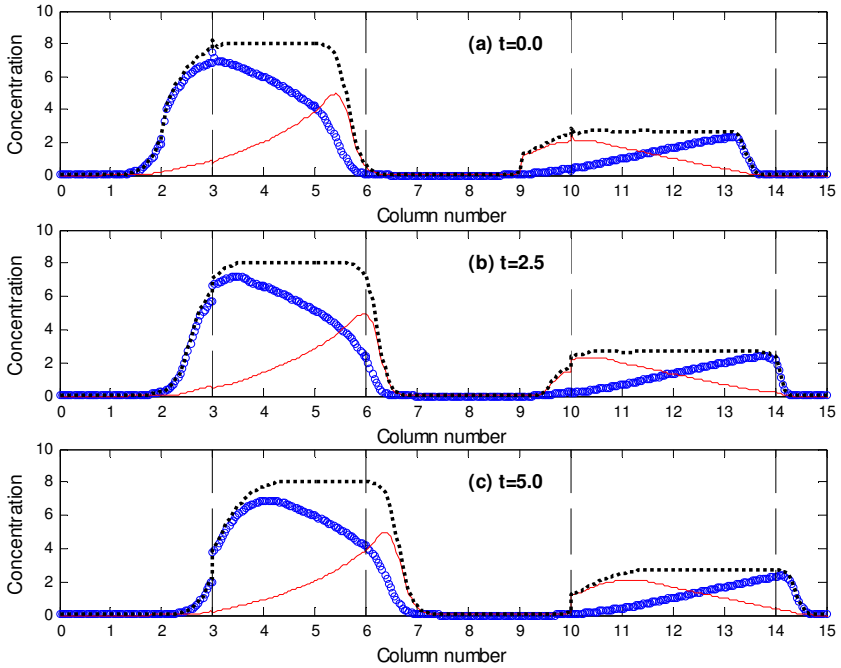

Fig. 6 Liquid concentration distribution of Ca^{2+}-H^+ ions (circles), K^+ ions (solid line) and total concentration (dotted line) over 15 columns at three different times within one 5 min cycle (v=*0.6*, N_m=*26* and N_{shift}=*53*).

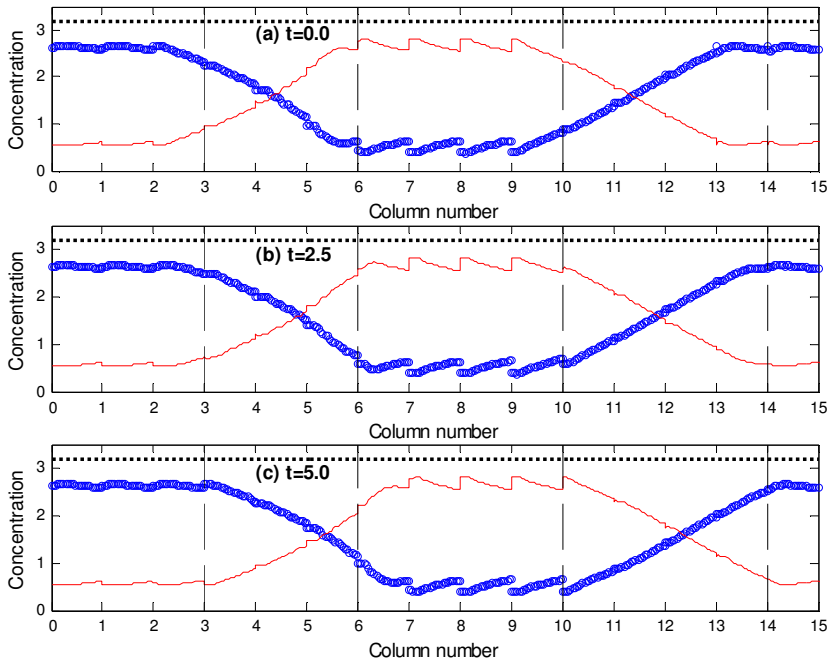

Fig. 7 Solid concentration distribution of Ca^{2+}-H^+ ions (circles), K^+ ions (solid line) and total concentration (dotted line) over 15 columns at three different times within one cycle (v=*0.6*, N_m=*26* and N_{shift}=*53*).

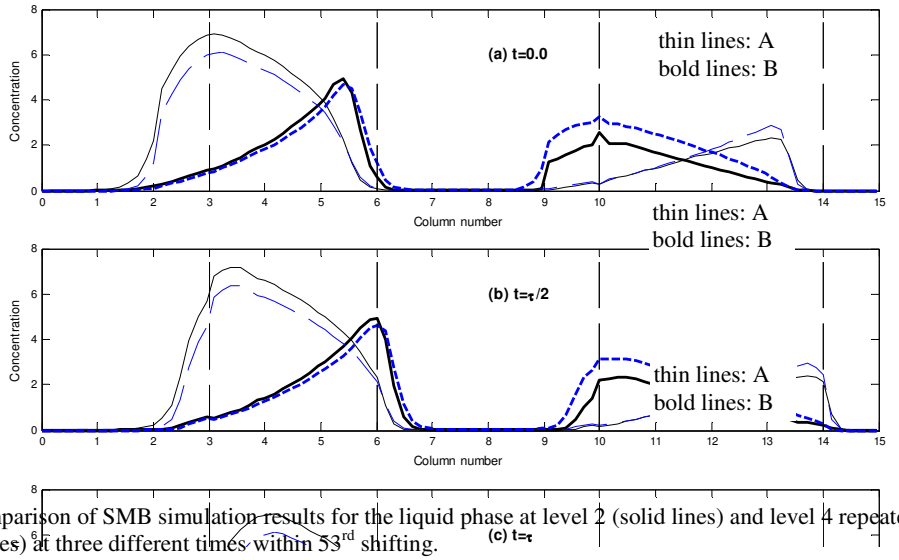

Fig. 8 Comparison of SMB simulation results for the liquid phase at level 2 (solid lines) and level 4 repeated (dashed lines) at three different times within 53rd shifting.

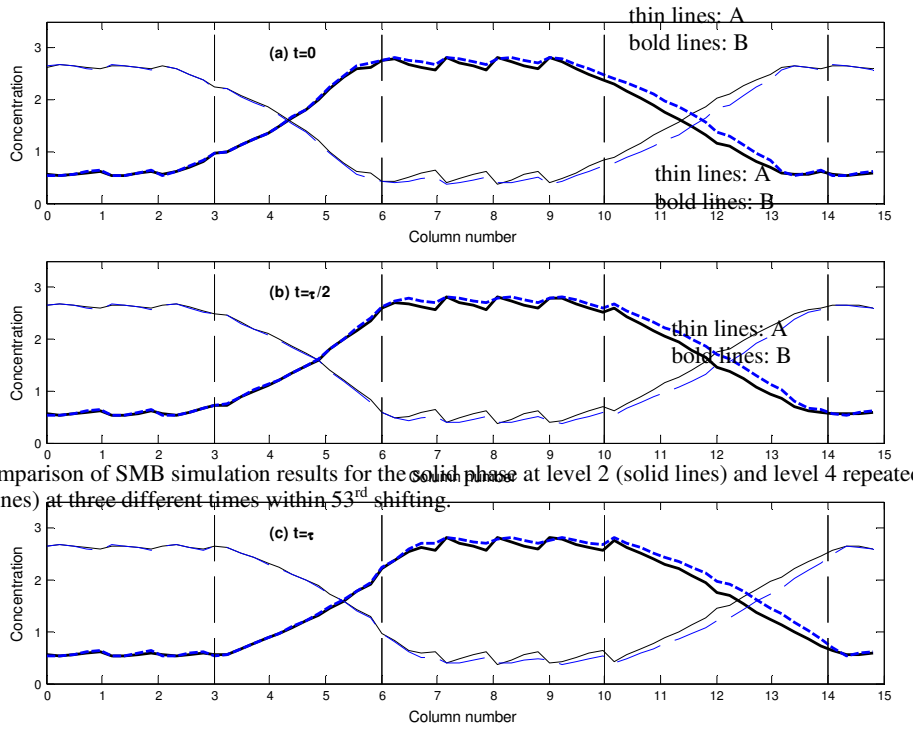

Fig. 9 Comparison of SMB simulation results for the solid phase at level 2 (solid lines) and level 4 repeated (dashed lines) at three different times within 53rd shifting.

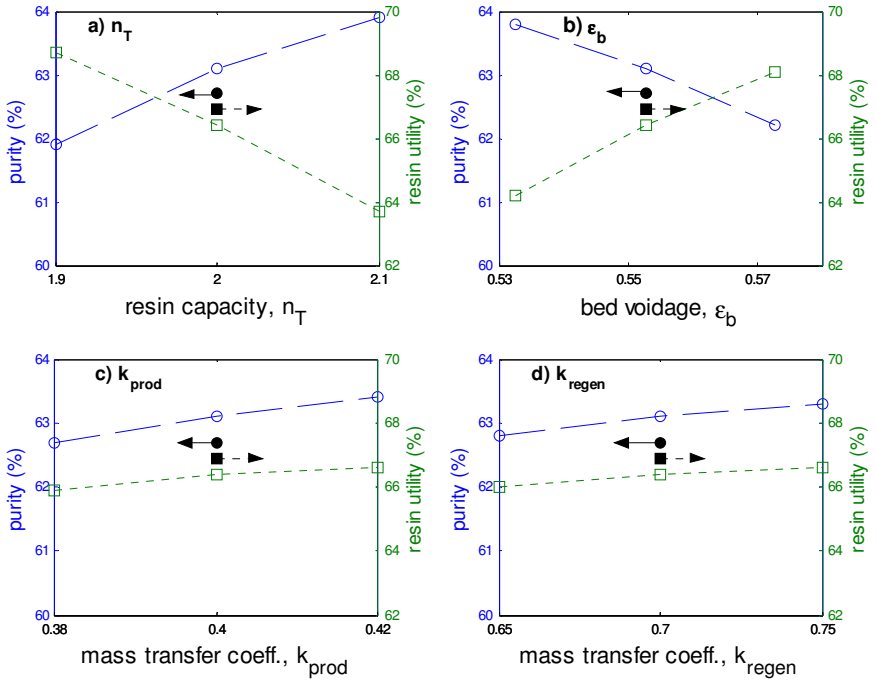

Fig. 10 Variation of purity in FS (circles) and resin utility (squares) with model parameters (filled circles and filled squares are experimental points).